Relationships Between Ψ_B-Energy Operator and Some Time-Frequency Representations

Abdel-Ouahab Boudraa, *Senior Member, IEEE*

***Abstract*—Ψ_B operator is an energy operator that measures the interactions between two complex signals. In this letter, new properties of Ψ_B operator are presented. Connections between Ψ_B operator and some time-frequency representations (cross-ambiguity function, short-time Fourier transform, Zak transform, and Gabor coefficients) are established. Link between Ψ_B operator of two input signals and their cross-spectrum is also derived. For two equal input signals, we find that Fourier transform of Ψ_B operator is proportional to the second derivative of the ambiguity function. The established links show the ability of Ψ_B operator to analyze nonstationary signals. A numerical example is provided for illustrating how to estimate the second order moment, of a FM signal, using Ψ_B operator. We compare the result to the moment given by the Wigner Ville distribution.**

***Index Terms*—Ψ_B energy operator, cross-ambiguity, cross-spectrum, Gabor coefficients, short-time Fourier transform.**

I. Introduction

THE Ψ_B Operator has been introduced to analyze the interaction between two signals [1], [2]. This operator is an extension of the cross Teager-Kaiser operator [3] to deal with complex signals [1]. We have recently shown how Ψ_B operator can be used for segmentation of dynamic nuclear cardiac images [4], transient detection [5], time delay estimation [6] and time series analysis [7]. Ψ_B operator is defined by [1]

$$\begin{aligned}&\Psi_B(x(t),y(t))\\&\quad=[0.5\dot{x}(t)\dot{y}^*(t)-0.25(\ddot{x}(t)y^*(t)+x(t)\ddot{y}^*(t))]\\&\qquad+[0.5\dot{x}^*(t)\dot{y}(t)-0.25(\ddot{x}^*(t)y(t)+x^*(t)\ddot{y}(t))].\end{aligned}\tag{1}$$

Let $R_{xy}(t,\tau)$ be the instantaneous Cross Correlation (CC) of $x(t)$ and $y(t)$:

$$R_{xy}(t,\tau)=x\left(t+\frac{\tau}{2}\right)\cdot y^*\left(t-\frac{\tau}{2}\right).\tag{2}$$

The output of Ψ_B is related to $R_{xy}(t,\tau)$ as follows [1]:

$$\Psi_B(x(t),y(t))=-\frac{\partial^2 R_{xy}(t,\tau)}{\partial\tau^2}\bigg|_{\tau=0}-\frac{\partial^2 R^*_{xy}(t,\tau)}{\partial\tau^2}\bigg|_{\tau=0}.\tag{3}$$

For $x(t)=y(t)$ the notation $\Psi_B(x(t),y(t))\equiv\Psi_B(x(t))$ is used. Examination of (3) shows that Ψ_B is a cross-energy function of two signals. Thus, links to transforms using the concept of instantaneous CC, such as Time-Frequency Representations (TFRs), can be found. In this letter new properties of Ψ_B are introduced. We show how some TFRs [Gabor Coefficients (GC), Short-Time Fourier Transform (STFT), Ambiguity Function (AF), and Zak Transform (ZT)] which are fundamentally similar and their application domains quite different, are related to Ψ_B. These links show that Ψ_B can be useful for nonstationary signals analysis.

II. Short-Time Fourier Transform

STFT is a classical TFR which allows one to obtain localized information of time and frequency of a signal. This transform is constructed by first choosing an analysis window, $x^*(t-a)$, and then compute the Fourier Transform (FT) of the windowed signal $y(t)$ [8]:

$$\psi_{xy}(a,b)=\int y(t)x^*(t-a)e^{-2j\pi tb}dt\tag{4}$$

where a and b are the delay and the modulation parameters. To relate Ψ_B to STFT, we recall the link between Ψ_B and the cross Wigner–Ville Distribution (WVD)[1], $W_{xy}(t,\nu)$ [1]:

$$\begin{aligned}&\Psi_B(x(t),y(t))\\&\quad=4\pi^2\int\nu^2\left(W_{xy}(t,\nu)+W^*_{xy}(t,\nu)\right)d\nu\\&\text{where } W_{xy}(t,\nu)\\&\quad=\int R_{xy}(t,\tau)e^{-2j\pi\nu\tau}d\tau.\end{aligned}\tag{5,6}$$

Let $x(t)$ and $y(t)$ be two complex signals. Ψ_B is linked to STFT by

$$\Psi_B(x(t),y(t))=8\pi^2\int\nu^2\left[\psi_{y\_x}(2t,2\nu)+\psi_{y^*\_x^*}(2t,2\nu)\right]\times e^{4j\pi\nu t}d\nu\tag{7}$$

where $y_-(t')=y(-t')$

Proof: We set $u=t+\tau/2$ in (6) and we obtain

$$W_{xy}(t,\nu)=2e^{4j\pi\nu t}\int x(u)y^*(2t-u)e^{-2j\pi u(2\nu)}du.\tag{8}$$

If we set $y_-(t')=y(-t')$, (8) simplifies to

$$W_{xy}(t,\nu)=2e^{4j\pi\nu t}\psi_{y\_x}(2t,2\nu).\tag{9}$$

Using the same setting and the conjugate version of (6) we obtain

$$W_{x^*y^*}(t,\nu)=2e^{4j\pi\nu t}\psi_{y^*\_x^*}(2t,2\nu).\tag{10}$$

Summing (9) and (10) and using (5) complete the proof. For $x(t)=y(t)$ being real signals, (7) is reduced to

$$\Psi_B(x(t))=16\pi^2\int\nu^2\psi_{x\_x}(2t,2\nu)e^{4j\pi\nu t}d\nu.\tag{11}$$

[1]All integrals are from $-\infty$ to $+\infty$ unless otherwise stated.

Manuscript received January 05, 2010; revised February 27, 2010. Date of publication March 15, 2010; date of current version April 21, 2010. The associate editor coordinating the review of this manuscript and approving it for publication was Dr. Alfred Mertins.

The author is with the IRENav, Ecole Navale, BCRM Brest, 29240 Brest Cedex 9, France (e-mail: boudra@ecole-navale.fr).

Color versions of one or more of the figures in this paper are available online at http://ieeexplore.ieee.org.

Digital Object Identifier 10.1109/LSP.2010.2045548

Equations (7) and (11) show that time resolution changes by a factor of 2. Thus, spacing of Ψ_{B} is quite large compared to the range of evaluation points for the STFT. Since the second order moment does not have a scaling factor in time and frequency, a well defined sampling grid must be used. If νt is integer, (11) is reduced to (12) which corresponds to the second order moment in frequency of the STFT where the window is chosen to be the time-reversed input signal:

$$\Psi_{\mathrm{B}}\left(x\left(\frac{t}{2}\right)\right) = 2\pi^2 \int (-1)^{\nu t}\nu^2 \psi_{x\_x}(t,\nu)d\nu. \tag{12}$$

III. Gabor Coefficients

GC is a signal analysis tool, for example, to process textured images. Using an analyzing function, $\gamma(t)$, and for a given input signal $f(t)$, GC are defined as follows :

$$C_{m,n} = \int f(t+n)\gamma^*(t)e^{-2j\pi mt}dt. \tag{13}$$

Let $x(t)$ and $y(t)$ be two complex signals. Ψ_{B} operator is related to GC by

$$\Psi_{\mathrm{B}}(x(t),y(t)) = 8\pi^2 \int \nu^2 \left[C_{2\nu,2t} + C^*_{-2\nu,2t}\right] e^{-4j\pi\nu t}d\nu \tag{14}$$

where $\gamma(t') = y(-t')$

Proof: Using the same reasoning as for the STFT with $u = \tau/2 - t$ we have

$$W_{xy}(t,\nu) = 2e^{-4j\pi\nu t}C_{2\nu,2t} \tag{15}$$

$$W_{x^*y^*}(t,\nu) = 2e^{-4j\pi\nu t}C^*_{-2\nu,2t}. \tag{16}$$

Summing (15) and (16) and using relation (5), we derive the relation (14). If the signal is sampled in both time and frequency with well defined sampling grid such that $m = 2\nu$ and $n = 2t$, we can rewrite (14) as

$$\begin{aligned}&\Psi_{\mathrm{B}}(x(t),y(t))\\ &\quad = 8\pi^2 \int \nu^2\left[C_{2\nu,2t} + C^*_{-2\nu,2t}\right]d\nu\\ &\Psi_{\mathrm{B}}\left(x\left(\frac{n}{2}\right), y\left(\frac{n}{2}\right)\right)\\ &\quad \approx 2\pi^2 \sum_m (-1)^{mn}m^2\left[C_{m,n} + C^*_{-m,n}\right].\end{aligned} \tag{17}$$

For $x(t) = y(t)$ being real signals, relation (17) is reduced to

$$\Psi_{\mathrm{B}}(x(t)) = 16\pi^2 \int \nu^2 C_{2\nu,2t}d\nu \tag{18}$$

$$\Psi_{\mathrm{B}}\left(x\left(\frac{n}{2}\right)\right) \approx 4\pi^2 \sum_m (-1)^{mn}m^2 C_{m,n}. \tag{19}$$

Spacing of Ψ_{B} is quite large compared to the range of evaluation points for GC. Equation (18) shows that Ψ_{B} corresponds to the second order moment of GC. The spacing of the GC and the STFT are large compared to the range of evaluation points for Ψ_{B}. This has a direct effect on the application for which each is best suited. Both the GC and the STFT are useful where there is a large amount of data, which must be analyzed at some coarser resolution (feature extraction task as part of a larger image analysis problem) [9]. Thus, in this case Ψ_{B} is an efficient and a simple way to calculate the second moment in frequency of both GC and STFT.

IV. Cross Ambiguity Function

Cross AF (CAF) is a TFR that is useful in many signal communication systems. CAF is given by:

$$A_{xy}(u,\tau) = \int R_{xy}(t,\tau)e^{-j2\pi ut}dt. \tag{20}$$

Let $\Gamma_{xy}(u,\nu)$ be the FT, $\mathcal{F}$, of $A_{xy}(u,\tau)$ with respect to τ

$$R_{xy}(t,\tau) \overset{t}{\longleftrightarrow} A_{xy}(u,\tau) \overset{\tau}{\longleftrightarrow} \Gamma_{xy}(u,\nu) \tag{21}$$

where $\Gamma_{xy}(u,\nu)$ represents the 2-D FT of $R_{xy}(t,\tau)$ and is the cross spectrum of $x(t)$ and $y(t)$. $A_{xy}(u,\tau)$ is expressed in terms of the FTs $X(\nu)$ and $Y(\nu)$ of $x(t)$ and $y(t)$ respectively as

$$\begin{aligned}A_{xy}(u,\tau) &= \int \Gamma_{xy}(u,\nu)e^{j2\pi\tau\nu}d\nu\\ &= \int X\left(\nu + \frac{u}{2}\right)Y^*\left(\nu - \frac{u}{2}\right)e^{j2\pi\tau\nu}d\nu.\end{aligned} \tag{22}$$

Let $x(t)$ and $y(t)$ be two complex signals. Ψ_{B} is related to $\Gamma_{xy}(u,\nu)$ by

$$\begin{aligned}&\mathcal{F}\{\Psi_{\mathrm{B}}(x(t),y(t))\}(u) =\\ &\qquad 4\pi^2 \int \nu^2\left[\Gamma_{xy}(u,\nu) + \Gamma^*_{xy}(-u,-\nu)\right]d\nu.\end{aligned} \tag{23}$$

Proof: According to (21), $R_{xy}(t,\tau)$ can be rewritten as

$$R_{xy}(t,\tau) = \int\int \Gamma_{xy}(u,\nu)e^{j2\pi(ut+\nu\tau)}dud\nu. \tag{24}$$

Differentiating twice both sides of $R_{xy}(t,\tau)$ and $R^*_{xy}(t,\tau)$ with respect to τ one gets

$$\begin{aligned}&\left.\frac{\partial^2 R_{xy}(t,\tau)}{\partial\tau^2}\right|_{\tau=0}\\ &\quad = -4\pi^2 \int\int \nu^2\Gamma_{xy}(u,\nu)e^{j2\pi ut}dud\nu\end{aligned} \tag{25}$$

$$\begin{aligned}&\left.\frac{\partial^2 R^*_{xy}(t,\tau)}{\partial\tau^2}\right|_{\tau=0}\\ &\quad = -4\pi^2 \int\int \nu^2\Gamma^*_{xy}(-u,-\nu)e^{j2\pi ut}dud\nu.\end{aligned} \tag{26}$$

Summing (25) and (26) and using (3) followed by FT complete the proof. FT of Ψ_{B} is also linked to CAF by

$$\begin{aligned}&\mathcal{F}\{\Psi_{\mathrm{B}}(x(t),y(t))\}(u) =\\ &\qquad -\frac{\partial^2}{\partial\tau^2}\left[A_{xy}(u,\tau) + A^*_{xy}(-u,\tau)\right]_{\tau=0}.\end{aligned} \tag{27}$$

Proof: According to (20) $R_{xy}(t,\tau)$ can be written as

$$R_{xy}(t,\tau) = \int A_{xy}(u,\tau)e^{j2\pi ut}du. \tag{28}$$

Differentiating twice both sides of (28) and its conjugate version we get

$$\left.\frac{\partial^2 R_{xy}(t,\tau)}{\partial\tau^2}\right|_{\tau=0} = \int \left.\frac{\partial^2 A_{xy}(u,\tau)}{\partial\tau^2}\right|_{\tau=0} e^{j2\pi ut}du \tag{29}$$

$$\left.\frac{\partial^2 R^*_{xy}(t,\tau)}{\partial\tau^2}\right|_{\tau=0} = \int \left.\frac{\partial^2 A^*_{xy}(-u,\tau)}{\partial\tau^2}\right|_{\tau=0} e^{j2\pi ut}du. \tag{30}$$

Using (3) we obtain

$$\Psi_B(x(t),y(t)) = -\int \underbrace{\frac{\partial^2}{\partial\tau^2}\Big[A_{xy}(u,\tau)+A^*_{xy}(-u,\tau)\Big]_{\tau=0}}_{H(u)} \times e^{j2\pi ut}du. \quad (31)$$

Observe from (31) that Ψ_B is the inverse FT of $H(u)$.

For $x(t)=y(t)$ being complex signals we have

$$\mathcal{F}\{\Psi_B(x(t))\}(u) = -2\frac{\partial^2 A_{xx}(u,\tau)}{\partial\tau^2}\Big|_{\tau=0}. \quad (32)$$

Proof: Using (2) it is easy to see that for $x(t)=y(t)$

$$\frac{\partial^2 R_{xx}(t,\tau)}{\partial\tau^2}\Big|_{\tau=0} = \frac{\partial^2 R^*_{xx}(t,\tau)}{\partial\tau^2}\Big|_{\tau=0} \quad (33)$$

and it follows from (29) and (30) that

$$\frac{\partial^2 A_{xx}(u,\tau)}{\partial\tau^2}\Big|_{\tau=0} = \frac{\partial^2 A^*_{xx}(-u,\tau)}{\partial\tau^2}\Big|_{\tau=0}. \quad (34)$$

Using (31) with $x(t)=y(t)$ one gets

$$\int \Psi_B(x(t))e^{-j2\pi ut}dt = -2\frac{\partial^2 A_{xx}(u,\tau)}{\partial\tau^2}\Big|_{\tau=0} \quad (35)$$

which completes the proof.

Computing FT of Ψ_B is identical to computing the second derivative, with respect to τ, of the CAF. Equation (23) shows another link of the FT of Ψ_B which is equal to the second order moment in frequency of the cross spectrum of the two input signals. Equation (32) gives the link between Ψ_B and AF.

V. Zak Transform

ZT is a mixed TFR of a signal that has relationships with the WVD, the Rihaczek distribution, and the Radar AF [10]. For $\alpha \geq 0$, ZT of f, $Z_\alpha f$, is a function on $\mathbb{R}^{2d}$:

$$Z_\alpha f(x,y) = \sum_{k\in\mathbb{Z}} f(x-\alpha k)e^{-2j\pi\alpha ky}. \quad (36)$$

In this work, we use the ZT with $\alpha=1, d=1$, which is denoted by $Z_f(x,y)$. The CAF of $f(t)$ and $g(t)$ can be computed directly from ZTs $Z_f(x,y)$ and $Z_g(x,y)$:

$$A_{fg}(u,\tau) = \int_0^1\int_0^1 Z_f(x,y)Z^*_g(x+\tau,y+u)e^{-2j\pi xu}dxdy. \quad (37)$$

Let $f(t)$ and $g(t)$ be two complex signals. Ψ_B is related to the ZT by

$$\Psi_B(f(t),g(t)) = \int_{-\infty}^{+\infty}\int_0^1\int_0^1 (Z_f(x,y)\ddot{Z}^*g(x,y+u) + Z^*_f(x,y)\ddot{Z}_g(x,y-u))e^{-2j\pi u(x-t)}dxdydu. \quad (38)$$

Proof: Differentiating twice both sides of (37) and its conjugate version with respect to τ we get

$$\frac{\partial^2 A_{fg}(u,\tau)}{\partial\tau^2}\Big|_{\tau=0} = \int_0^1\int_0^1 Z_f(x,y)\ddot{Z}^*_g(x,y+u)e^{-2j\pi xu}dxdy \quad (39)$$

$$\frac{\partial^2 A^*_{fg}(u,\tau)}{\partial\tau^2}\Big|_{\tau=0} = \int_0^1\int_0^1 Z^*_f(x,y)\ddot{Z}_g(x,y-u)e^{-2j\pi xu}dxdy. \quad (40)$$

Substituting (39) and (40) in (31) completes the proof where $\ddot{Z}_g(x,y+u) = \partial^2 Z_g(x+\tau,y\pm u)/\partial\tau^2|_{\tau=0}$. If $f(t)=g(t)$, (38) is reduced to

$$\Psi_B(f) = 2\int_{-\infty}^{+\infty}\int_0^1\int_0^1 Z_f(x,y)\ddot{Z}^*g(x,y+u) \times e^{-2j\pi u(x-t)}dxdydu. \quad (41)$$

The AF on the integer lattice is defined as

$$A_{ff}(n,m) = \int_0^1\int_0^1 \mid Z_f(x,y)\mid^2 e^{2j\pi(-mx+ny)}dxdy. \quad (42)$$

Using (32) it is easy to show that

$$\mathcal{F}\{\Psi_B(x(t))\}(n) = 8\pi^2\int_0^1\int_0^1 x^2(t)\mid Z_f(x,y)\mid^2 e^{2j\pi ny}dxdy. \quad (43)$$

Equations (38), (41), and (43) reveals links between ZT and Ψ_B.

VI. Results

We show how Ψ_B can be used to estimate the second order moment in frequency, $\langle\nu^2\rangle_t$, of an FM signal, which is a useful feature for signal classification. Using (5), the moment $\langle\nu^2\rangle_t$ of a signal $y(t)$ is given by

$$\langle\nu^2\rangle_t = \frac{\int\nu^2 W_y(t,\nu)d\nu}{\mid y(t)\mid^2} \quad (44)$$

$$\langle\nu^2\rangle_t = \frac{\Psi_B(y(t))}{8\pi^2\mid y(t)\mid^2} \quad (45)$$

where $\mid y(t)\mid^2 = \int W_y(t,\nu)d\nu$. Let $y(t)$ be a noisy version of LFM signal, $x(t)=e^{2j\pi\phi(t)}$, defined by

$$y(t) = x(t)+n(t) \quad (46)$$

$\phi(t)=\alpha t^2+\beta t+c$. $n(t)$ is a Gaussian noise, $\mathcal{N}(0,\sigma^2)$. This complex noise consists of independent real and imaginary parts. The WVD of $x(t)$ is a Dirac function concentrated along its instantaneous frequency, $\nu_x(t)=2\alpha t+\beta$:

$$W_x(t,\nu) = \delta(\nu-\beta-2\alpha t). \quad (47)$$

Since $\mid x(t)\mid^2 = 1$ and putting (47) in (44) we obtain

$$\langle\nu^2\rangle_t = (2\alpha t+\beta)^2. \quad (48)$$

To illustrate the computation of $\langle\nu^2\rangle_t$, we consider a signal $y(t)$ with parameters ($\alpha=50, \beta=25, c=10$) where $t\in[0,1.2]$, sampled at $T=5.10^{-4}$ and with different SNRs. We compare the true value of $\langle\nu^2\rangle_t$ [(48)] and the numerical estimations by WVD [(44)] and Ψ_B [(45)]. Operator Ψ_B is implemented using symmetric finite difference scheme [6]. WVD displayed in Fig. 1, clearly reveals the features of the noisy signal $y(t)$ (SNR = 40 dB). Results of $\langle\nu^2\rangle_t$, by Ψ_B and WVD, from 600 runs Monte-Carlo simulations are shown in Figs. 2 and 3. Origin of time axis is shifted to -0.1 sec for displaying purpose. Although the match of the moments $\langle\nu^2\rangle_t$ is not perfect, Ψ_B

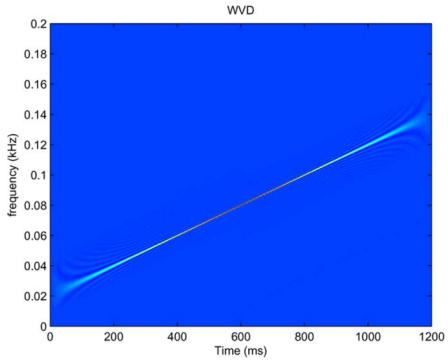

Fig. 1. WVD of noisy signal $y(t)$ ($\mathrm{SNR} = 40$ dB).

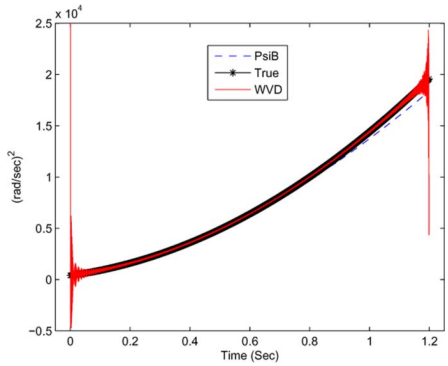

Fig. 2. Moment $\langle \nu^2 \rangle_t$ of $y(t)$ ($\mathrm{SNR} = \infty$). (Black star) True, (blue dashed line) Ψ_B, and (red solid line) WVD.

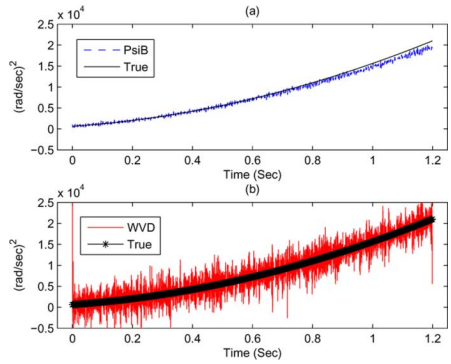

Fig. 3. Moment $\langle \nu^2 \rangle_t$ of $y(t)$ ($\mathrm{SNR} = 40$ dB). (Black) True, (blue dashed line) Ψ_B, and (red solid line) WVD .

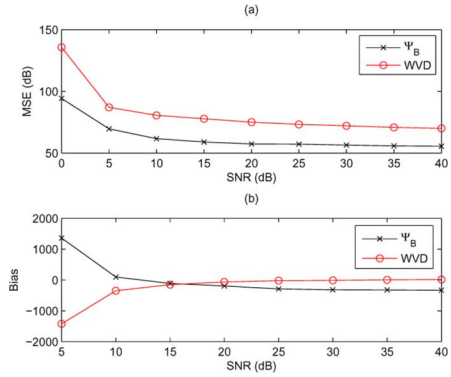

Fig. 4. (a) MSEs (dB) in $\langle \nu^2 \rangle_t$ estimation for Ψ_B and WVD. (b) Bias in $\langle \nu^2 \rangle_t$ estimation for Ψ_B and WVD.

shows a good match (Fig. 2) and with little oscillations due to noise [Fig. 3(a)]. Fig. 2 also shows an agreement of the WVD moment with the true value but with fluctuations of high magnitude at the beginning and the end of free-noise signal $x(t)$. These fluctuations are due to the effect of the broad frequency spread observed on the beginning and on the end of the signal $y(t)$ (Fig. 1). For noisy signal, these fluctuations are very high over all the signal [Fig. 3(b)]. In Fig. 4(a), we plot the MSEs in $\langle \nu^2 \rangle_t$ estimation versus the SNRs for both Ψ_B and WVD. As seen in Fig. 4(a), across a range of different SNRs, Ψ_B provides a good performance over the WVD. Bias measures reported in Fig. 4(b) show that both Ψ_B and WVD are less biased for SNR > 15 dB but the little bias is achieved by WVD. Due to its localization property, Ψ_B is sensitive in very noisy environment compared to WVD, however it offers a significant computation advantage over WVD. Cost of calculating Ψ_B is very small compared to WVD. In general, Ψ_B gives interesting results provided that $\Psi_B(n(t)) \simeq -2\Psi_B(x(t), n(t))$. Also, attention must be given to discretization of Ψ_B.

VII. Concluding Remarks

The main point of this letter is to establish links between Ψ_B and some TFRs. Even the studied TFRs have different application domains, they are all related to Ψ_B. Lemmas 1 and 2 show that time resolution changes by a factor of 2. Thus, the spacing of Ψ_B is quite large compared to the range of evaluation points for both STFT and GC. Connections between ZT and Ψ_B are also derived. The established links show the interest of Ψ_B to analyze nonstationary signals. Particularly relation (18) shows that Ψ_B corresponds to the second order moment in frequency of GC. We have established the link between the FT of Ψ_B of two input signals and the second order moment of the cross-spectrum. For two equal input signals we find that the FT of Ψ_B is proportional to the second derivative of the AF. Preliminary results show that Ψ_B is effective for estimating the second order frequency moment of a signal.

References

[1] J. C. Cexus and A. O. Boudraa, "Link between cross-Wigner distribution and cross-Teager energy operator," *Electron. Lett.*, vol. 40, no. 12, pp. 778–780, 2004.

[2] A. O. Boudraa, J. C. Cexus, K. Abed-Meraim, and Z. Saidi, "Interaction measure of AM-FM signals by cross-Ψ_B-energy operator," in *Proc. IEEE ISSPA*, 2005, pp. 775–778.

[3] J. F. Kaiser, "Some useful properties of Teager's energy operators," *Proc. ICASSP*, vol. 3, pp. 149–152, 1993.

[4] A. O. Boudraa, J. C. Cexus, and H. Zaidi, "Functional segmentation of dynamic nuclear medicine images by cross-Ψ_B-energy operator," *Comput. Meth. Prog. BioMed.*, vol. 84, no. 2–3, pp. 146–152, 2006.

[5] A. O. Boudraa, S. Benramdane, J. C. Cexus, and T. Chonavel, "Some useful properties of cross-Ψ_B-energy operator," *Int. J. Electron. Commun.*, vol. 63, no. 9, pp. 728–735, 2009.

[6] A. O. Boudraa, J. C. Cexus, and K. Abed-Meraim, "Cross-Ψ_B-energy operator-based signal detection," *J. Acoust. Soc. Amer.*, vol. 123, no. 6, pp. 4283–4289, 2008.

[7] A. O. Boudraa, J. C. Cexus, M. Groussat, and P. Brunagel, "An energy-based similarity measure for time series," *Adv. Signal Process.*, 2008.

[8] A. Mertins, *Signal Analysis: Wavelets, Filter Banks, Time-Frequency Transforms and Applications*. Chichester, U.K: Wiley, 1999.

[9] M. R. Dellomo and G. M. Jacyna, "Wigner transforms, Gabor coefficients, and Weyl-Heisenberg wavelets," *J. Acoust. Soc. Amer.*, vol. 89, no. 5, pp. 2355–2361, 1991.

[10] A. J. E. M. Janssen, "The Zak transform: A signal transform for sampled time-continuous signals," *Philips J. Res.*, vol. 43, pp. 23–69, 1995.